


# Multi-Wavelength Polarizer Based on Metal Grating-Assisted Microstructured Fiber

Jiexuan Gu , Boyao Li , Changming Xia, Zhiyun Hou, and Guiyao Zhou , *Senior Member, IEEE*

**Abstract**—Multi-wavelength polarizers have many essential applications in optics, quantum communication, Q switch and relating research fields. However, polarizing waveband of the traditional polarizer is restricted in the structure of fibers, which results in finite polarizing wavelengths. In this work, a novel D-shaped microstructure fiber polarizer (DMFP) with metal grating was proposed. Utilizing the abundant harmonic vector characteristics on the surface of metal grating, the DMFP can realize the function of multi-band polarization filtering. Numerical results show that it can achieve three bands of polarization filtering in x-polarized mode from 350 nm to 1600 nm and the resonance wavelengths are periodically modulated by grating. In the meanwhile, by optimizing grating parameters, the number of bands of polarization filtering can be further increased, thus, it fulfills the effective adjustment of polarization filtering. It is promising that metal grating based DMFP has great potential values in the fields of optical filter, communication, and functional devices, etc.

**Index Terms**—Microstructure optical fiber, multi-band polarizing filter, metal grating.

## I. INTRODUCTION

**D**UE to its flexible and portable structure, optical fibers have a valuable application prospect in the field of communication, such as photoelectric modulators [1], [2], multiplexers [3] and polarizers [4], [5]. Further, to control the polarization, it has become a trend to use polarization multiplexers, polarization switches and polarization rotators in quantum communication and integrated optical system. Therefore, it is necessary to propose a novel polarization filter in the field of functional devices.

The field of polarization filtering technology has rapidly and considerable expanded during the past decades. As an optical phenomenon of free-electron light interaction on the metal surface, surface plasmon can be used to improve the performance of many devices, such as optical filters and polarization filters [6]–[8], etc. A hybrid plasmonic TE-pass polarizer has been

designed, which provides large extinction ratio with low insertion loss for the TE mode, firstly proposed by Alam in 2012 [9]. After four years, based on hybrid plasma waveguide, Sun reported an ultra-low insertion loss polarizer which has a very low insertion loss of less than 0.04 dB for the TE mode [10]. However, owing to the block property of the waveguide itself, these devices cannot be compatible with the existing optical fiber communication systems.

Therefore, it is essential to find a way to solve these problems and realize the polarization filtering in the field of optical fiber communication. Naturally, people combined surface plasmon resonance (SPR) characteristics with traditional single-mode fiber to achieve polarizing filtering. Wang *et al.* verified the polarization characteristics of the thin metal film plasmon-assisted fiber optic polarizer from both experimentally and theoretically in 2020 [11]. The polarizer can offer a high polarization extinction ratio (33.1 dB) and a low insertion loss (1.1 dB) and has excellent temperature stability in the range of  $-48$ – $82$  °C.

Compared with the traditional optical fiber, microstructure optical fiber (MOF) has its unique features and flexibilities. It is gradually found that a polarization filter can be obtained by filling or coating the metals, which can flexibly control the waveguiding properties. When phase matching occurs between the metal surface plasmon polariton (SPP) and the transmitted light, the coupling resonance phenomenon appears, which makes the loss of specific polarized mode greatly increase. In 2013, Xue *et al.* proposed a metal-coated polarization filter, the confinement loss (CL) of FWHM in a single polarization direction is only 20 nm [12]. In 2015, Liu *et al.* reported a broadband single-polarization MOF polarized filter based on SPR [13]. The loss of y-polarized mode is much higher than x-polarized mode in the wavelength range of 1.2–1.63  $\mu\text{m}$ . In 2016, Li *et al.* designed a polarization filter based on MOF with asymmetry around gold-coated holes, the loss can reach as high as 750 dB/cm in x-polarized [14]. Despite this superior performance, their functionality is restricted and can only achieve the polarization in a single direction and the number of polarization wavelengths is limited. To this end, in 2016, a polarization filter at the two communication windows based on MOF with two large-diameter gold-coated air holes is proposed. Numerical simulations reveal that it possesses high extinction ratios of 396 and  $-292$  dB at the two wavelengths, respectively [15]. Then, Lu *et al.* produced a metal-filled MOF polarization filter based on SPR, realizing dual-polarization at a single wavelength [16]. Nevertheless, the works above only solve the problem of single polarizing direction, and do not realize the dual modulation in

Manuscript received February 26, 2022; accepted April 2, 2022. Date of publication April 8, 2022; date of current version April 28, 2022. This work was supported in part by the Science and Technology Program of Guangzhou under Grant 2019050001 and in part by GDUPS (2017). (*Corresponding author: Guiyao Zhou.*)

Jiexuan Gu, Changming Xia, Zhiyun Hou, and Guiyao Zhou are with the Guangzhou Key Laboratory for Special Fiber Photonic Devices, South China Normal University, Guangzhou 510006, China, and also with the SCNU Qingyuan Institute of Science and Technology Innovation Company, Ltd., Qingyuan 511517, Guangdong, China (e-mail: 2020022294@m.scnu.edu.cn; xiacmm@126.com; houzhizyun@m.scnu.edu.cn; gyzhou@scnu.edu.cn).

Boyao Li is with the School of Electronic Engineering and Intelligentization, Dongguan University of Technology, Dongguan, Guangdong 523808, China (e-mail: liby@dgut.edu.cn).

Digital Object Identifier 10.1109/JPHOT.2022.3165214

multi-band. Although in 2017, Li *et al.* researched the dual-wavelength single-polarization filter based on MOF, and got high loss in the y-polarized at two communication windows [17]. However, the number of polarization filtering bands is restricted because the coupling resonance between SPP mode and core mode is limited due to the complicated form of end face of the MOF and the subtle adjustment of the fiber structure.

Subsequently, people investigated that the SPP model could be enriched by modifying the metal structure itself to increase the harmonic wave vector. In 2017, SEO *et al.* mentioned the SPR characteristics of metal gratings [18], using the incident angle and polarization state of light to represent the degree of optical coupling and the position of SPR peak. However, further reports on metal grating and fiber waveguide are less, so the problem of multi-band polarization filtering in fiber has not been solved.

In this paper, we present a metal grating-assisted D-shaped MOF filter that can achieve tunable multi-band polarization filtering. The theoretical results demonstrate that the x-polarized core mode is scattered by the MOF structure and then coupled with the mode existing in the metal grating. And the coupling period is related to the grating period, therefore, multi-wavelength polarization characteristics could be achieved. Further research indicates that more harmonic modes of the grating are coupled with the core mode due to the influence of grating parameters. Compared with the traditional SPR, the new coupling method can generate more polarization bands and break the limitation of single mode coupling. We believe that the DMFP with metal grating has great potential value in optical filtering, communication, functional devices, etc.

## II. STRUCTURE DESIGN

In order to get controllable multi-wavelength polarization filtering from visible light to near infrared, a metal (Au) grating-assisted D-shaped MOF was designed, as shown in Fig. 1(a). Firstly, following polishing, the D-shaped MOF is achieved. Then, taking the method of ion beam etching, the period-grating grooves can be obtained. In addition, the metal grating with plate can be formed on the D-shaped MOF with period grooves by means of magnetron sputtering. Finally, the multi-wavelength polarization filter can be achieved. And the related structure parameters are shown in Fig. 1(b). All air holes are arranged in a hexagonal arrangement with a lattice pitch ( $\Lambda$ ). Considering the structure flexibility and process feasibility, the diameter of the air hole ( $d$ ) is  $0.45\Lambda$ . It is worth noting that a proper duty ratio can ensure single-mode condition. A row of gratings is engraved on the D-shaped surface with the period ( $t$ ), the width ( $a$ ) and the height ( $H_m$ ) are 500 nm, 280 nm, and 200 nm, respectively. We consider using a metal plate to enhance the modulation depth of the grating and the thickness ( $Mt$ ) is 30 nm.

Using D-shaped MOF as the substrate, the coupling efficiency with grating can be improved, and it also provides a platform for grating etching. The function of the grating is to produce abundant wave vectors. When incident light strikes the diffraction grating, multiple integers of the grating vector can be added to or subtracted from the wave vector of the light via Bragg scattering. Based on this characteristic, the x-component of the

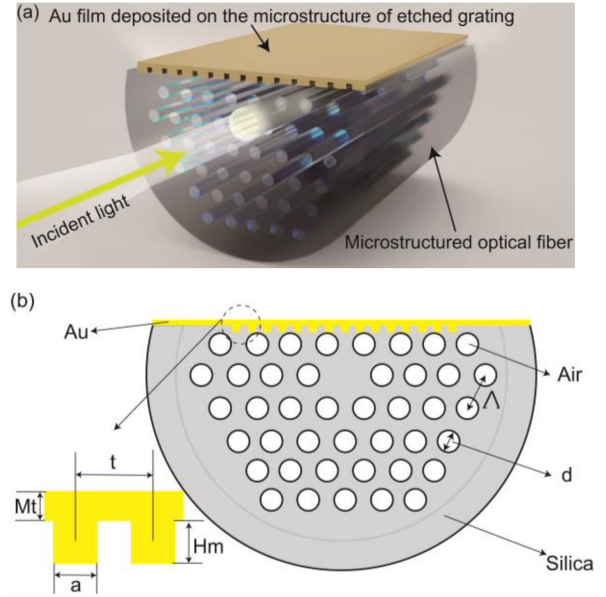


Fig. 1. (a) Schematic diagram of the device and (b) cross-sectional view of the related structure parameters.

wave vector is

$$K_{x'} = \frac{2\pi}{\lambda} \sin \theta \pm m \frac{2\pi}{t} \quad (1)$$

the y-component of the wave vector is

$$K_{y'} = \frac{2\pi}{\lambda} \cos \theta \quad (2)$$

Here  $\theta$  is the deflection angle to the surface normal of the grating grooves,  $m$  is an integer representing the diffraction order ( $m = \pm 1, \pm 2, \pm 3 \dots$ ), and  $\lambda$ , the wavelength in vacuum. Finally, the metal plate facilitates filtering by increasing the CL.

Considering the background materials is  $\text{SiO}_2$ , its dispersion performance can be described by Sellmeier equation [19]. The metal model can be analyzed by Drude Lorentz equation [20].

In addition, considering that the CL is a very essential parameter to describe polarizing performance, the loss can be calculated by the (3).

$$\alpha = 8.686 \times \frac{2\pi}{\lambda} \text{Im}[n_{eff}] (\text{dB/cm}) \quad (3)$$

Where  $\text{Im}[n_{eff}]$  denotes the imaginary part of the effective refractive index (RI).

## III. THEORETICAL ANALYSIS

Fig. 2(a), (b) indicate the CL in the x-polarized and y-polarized modes, respectively. Two surface plasmon resonances are observed near the wavelengths of 954 nm ( $\lambda_2$ ) and 1345 nm ( $\lambda_3$ ), resulting in sharp peak loss as shown in Fig. 2(a). The illustration in Fig. 2(a) presents the CL in the range of 350-700 nm, and maximum CL is observed at the location of 500 nm ( $\lambda_1$ ). As shown in Fig. 2(b), the CL can reach as high as 176 dB/cm in y-polarized mode, and it is more sensitive than the x-polarized mode. Based on these phenomena, it is deduced that both x-polarized and y-polarized modes interact with SPP, and

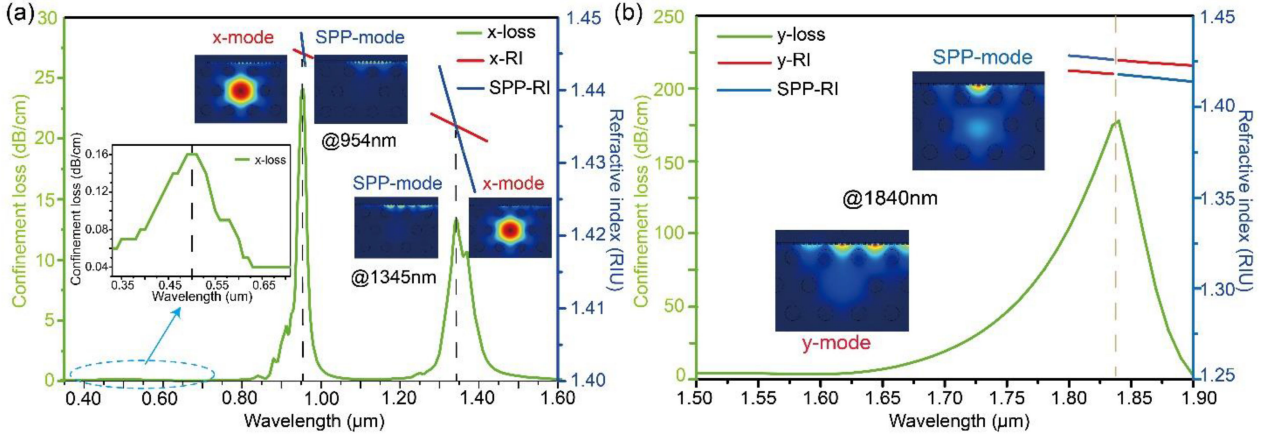


Fig. 2. (a) The coupling resonance between x-polarized mode and SPP. The illustration shows the CL in the visible wavelength region. (b) Coupling resonance between y-polarized mode and SPP.

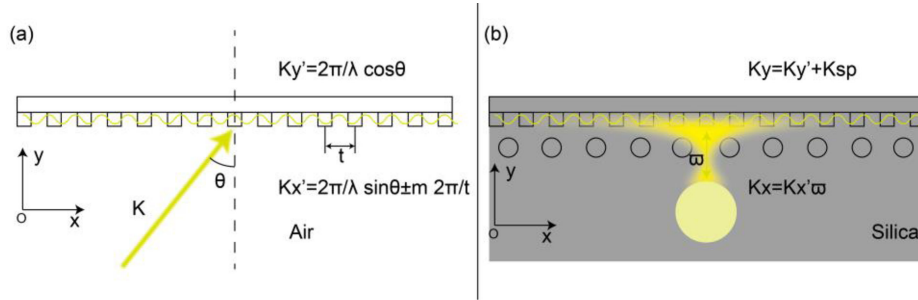


Fig. 3. The coupling mechanism (a) only have the grating. (b) between the fiber core and grating.

the coupled mode equation satisfies the following equations.

$$\frac{dE_1}{dz} = i\beta_1 E_1 + i\kappa E_2 \quad (4)$$

$$\frac{dE_2}{dz} = i\beta_2 E_2 + i\kappa E_1 \quad (5)$$

Where  $E_1$  and  $E_2$  express the mode fields of different modes, respectively.  $\beta_1$  and  $\beta_2$  are the propagation constants of corresponding modes.  $\kappa$  presents the strength of coupling and is the propagation constant of coupled mode after the coupling of two modes.

$$\beta_{\pm} = \frac{\beta_1 + \beta_2}{2} \pm \sqrt{\delta^2 + \kappa^2} \quad (6)$$

$$\delta = \frac{\beta_1 - \beta_2}{2} = \delta_r + i\delta_i \quad (7)$$

When the phase matching condition is satisfied,  $\delta_r = 0$ ,  $\delta^2 + \kappa^2 = -\delta_i^2 + \kappa^2$ . If  $\delta_i > \kappa$ , the real part of  $\beta_+$  and  $\beta_-$  is equal but the imaginary part is not. While  $\delta_i < \kappa$ , the imaginary part of  $\beta_+$  and  $\beta_-$  is equal but the real part is not, then, it can achieve complete coupling. As shown in the maximum loss region in Fig. 2(a), the real part of RI of x-polarized core mode and SPP mode are equal. On the contrary, in Fig. 2(b), its real part of the RI is not equal, and the real part of RI anti-cross occurs. It means the complete coupling happens between y-polarized core mode

and SPP mode. Therefore, it explains the phenomenon that the CL of y-polarized mode is greater than x-polarized mode in the phase matching regions.

Besides, the loss peak in y-polarized mode has only one, but the numbers of loss peak in x-polarized mode are more than y-polarized mode. The phenomenon is widely divergent from the previous D-shaped metallized fiber which only produces one loss peak [21]. It can be explained from the aspect of coupling between metal grating and fundamental. For x-polarized mode, the vibration direction of the electric field is perpendicular to the grating. It indicates that the x-polarized core mode is periodically modulated by the grating easily, and then coupled with the SPP wave on the other side of the grating. Based on this concept, in the x-polarized, multiple peaks appear at  $\lambda_1$ ,  $\lambda_2$  and  $\lambda_3$ . And  $\lambda_3 - \lambda_2 \approx \lambda_2 - \lambda_1 = kt$ , where  $k$  expresses the vector detuning and  $0 < k \leq 1$ . In vacuum, the vector detuning is 1. It is proved that the x-polarized mode is related to the grating modulation. However, it is not completely equal to the period because RI has subtle change at different wavelengths. Since the resonance characteristics of  $\lambda_2$  and  $\lambda_3$  are obvious, the following work is based on their analysis. Specifically, when the incident light is transmitted in the fiber core, the wave vector component in the x-polarized is generated, then it irradiates the diffraction grating. The component has a deflection angle  $\theta$  relative to the normal direction of the grating surface. Due to the Bragg scattering, the wave vector component in the x-polarized satisfies (1). And it is

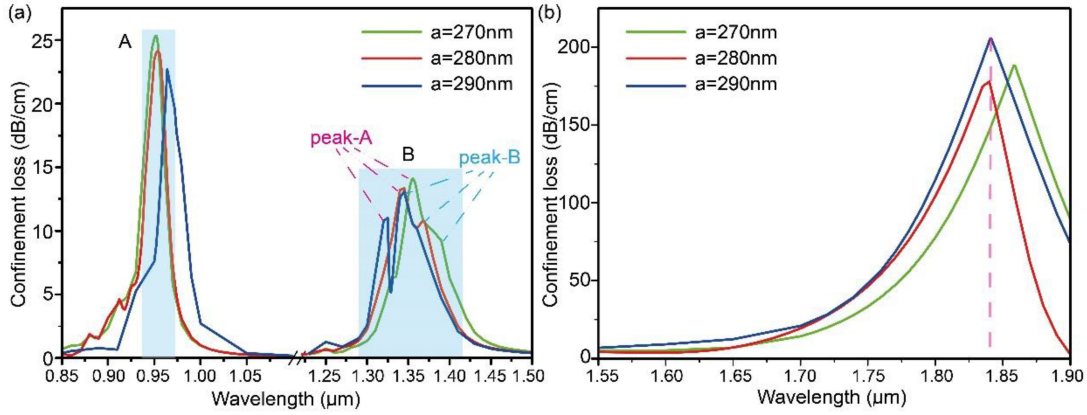


Fig. 4. The influence of grating width on the device,  $a$  represents the grating width. (a) The confinement loss of x-polarized mode. (b) The confinement loss of y-polarized mode with varying width from 270 to 290 nm.

also affected by the surrounding air holes, so it is not a simple wave vector matching. For describing the results, a new variable is introduced, vector matching detuning ( $\varpi$ ), and  $|\varpi| \leq 1$ , (1) then becomes

$$\beta_{core,x} = K_{x'}\varpi = \left( \frac{2\pi}{\lambda} \sin \theta \pm m \frac{2\pi}{t} \right) \varpi \quad (8)$$

The deduction indicates the maximum loss of x-polarized core mode is periodically modulated by grating.

On the other hand, affected by the diffraction grating, the wave vector component in the y-polarized satisfies (2). By solving the boundary conditions of the Maxwell equation, the dispersion relation of SPP propagating on the metal plate is described as

$$K_{sp} = \frac{\omega}{c} \sqrt{\frac{\varepsilon_d \varepsilon_m}{\varepsilon_d + \varepsilon_m}} \quad (9)$$

In the y-polarized, the conservation of momentum can be achieved if the surface plasmon wave vector in core mode equals the wave vector of the incident light on the metal surface, that is,  $\beta_{core,y} = K_{y'} + K_{sp}$ . This leads to the following relation.

$$\beta_{core,y} = \frac{2\pi}{\lambda} \cos \theta + \frac{\omega}{c} \sqrt{\frac{\varepsilon_d \varepsilon_m}{\varepsilon_d + \varepsilon_m}} \quad (10)$$

#### A. Influence of Grating Structure ( $a$ , $t$ )

The grating structure plays a key role in the performance of the device. To optimize optical properties, we simulate the parameters of the grating width and period. Fig. 4 represents the CL for changing width. For  $a$  of 270 nm, 280 nm, and 290 nm, respectively. As seen from Fig. 4(a), red-shifting of resonance wavelength A is noticeable from the profile and the corresponding peaks value reduces from 25.11 dB/cm to 22.68 dB/cm. It happens because the wave vector requires a higher wavelength to penetrate large grating width. It is also to be noticed that the larger grating width produces more damping to the evanescent field's potency. That is why CL also drops to a lower value with increasing width. Interestingly, in the long wavelength region (i.e., region B), the CL in y-polarized is significantly increase. Hence, there is the component of y-polarized participates in the coupling in the x-polarized. Then the x-component of the wave

vector is

$$\beta_x = \frac{2\pi}{\lambda} \sin \theta + m \frac{2\pi}{t} \quad (11)$$

The y-component of the wave vector is

$$\beta_y = \chi \bullet \frac{2\pi}{\lambda} \cos \theta \quad (12)$$

Here  $\chi$  is the component coefficient, and  $\chi \ll 1$

The dispersion relation of SPP propagating on the metal plate is described as

$$K_{sp} = \frac{\omega}{c} \sqrt{\frac{\varepsilon_d \varepsilon_m}{\varepsilon_d + \varepsilon_m}} \quad (13)$$

The coupling occurs when  $K_{sp} = \sqrt{\beta_x^2 + \beta_y^2}$  is satisfied, this leads to the following relation.

$$\sin \theta = -m \frac{\lambda}{t(1 - \chi^2)} \pm \frac{\sqrt{\left(m \frac{\lambda}{t}\right)^2 - (1 - \chi^2) \left[ \chi^2 - \frac{\varepsilon_d \varepsilon_m}{\varepsilon_d + \varepsilon_m} + \left(m \frac{\lambda}{t}\right)^2 \right]}}{1 - \chi^2} \quad (14)$$

Based on the derivation, the loss spectrum in region B becomes complex, and the loss peak splits, forming peak-A and peak-B. The value of peak-A is significantly decreased and the corresponding resonance wavelength appears a blue shift with the width increasing. Conversely, the value of peak-B is increased and the corresponding resonance wavelength shows a blue shift. It is noting that it occurs broadening phenomenon with the width decreasing. And it can be seen from the simulation results in Fig. 4(b), the resonance wavelength blue-shifts first and then fixes at 1840 nm with the width from 270 nm to 290 nm.

The influence of the grating period change on the CL of the device is shown in Fig. 5. The grating period is varied from 490 nm to 510 nm. Blue-shifting of resonance wavelength A and red-shifting of resonance wavelength B are noticeable from the Fig. 5(a). Interestingly, for 490 nm, 500 nm, and 510 nm, the value of  $\lambda_3 - \lambda_2$  is calculated about 380 nm, 389 nm, and 402 nm. Fig. 6 is analyzed its relationship with the grating period. The distinct increase phenomenon of the resonant wavelength

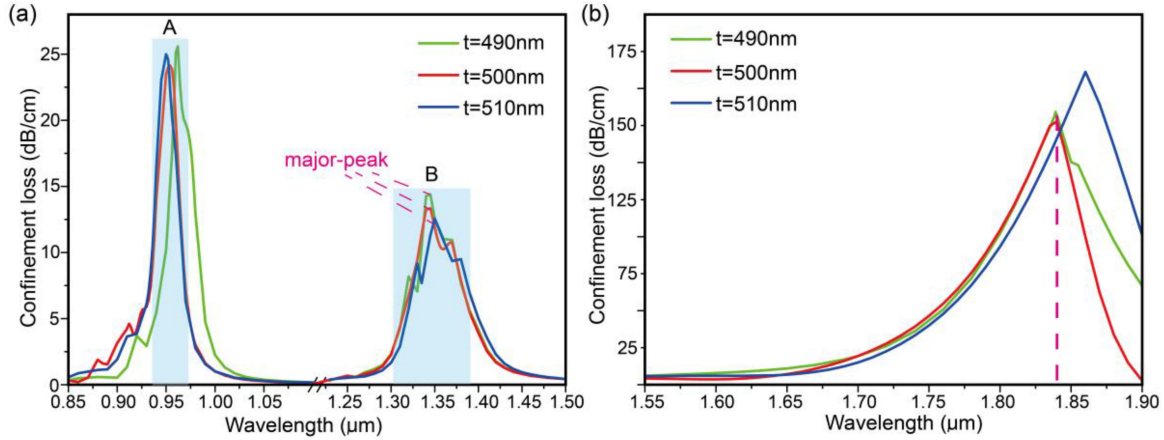


Fig. 5. The influence of grating period on the device,  $t$  represents the grating period. (a) The confinement loss of x-polarized mode. (b) The confinement loss of y-polarized mode with varying period from 490 to 510 nm.

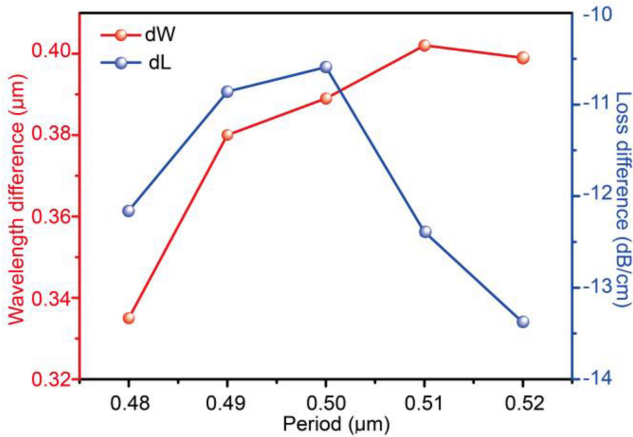


Fig. 6. The changes of confinement loss and wavelength shifts with the varieties of grating period.

difference is accompanied by the change of loss difference with the grating period increasing and the variable grating structure is the major reason of the change of loss difference. Due to the dispersion of materials change with the wavelength, then the vector detuning ( $k$ ) also changes with variety of wavelength. So, the movement of loss peak of coupling resonance is not linear. Based on this concept, the previous inference is proved which the x-polarized mode is related to the grating periodically modulation. Note that, in Fig. 5(b), the resonance wavelength fixes at 1838 nm first and then red-shifts. CLs are obtained about 184.18 dB/cm, 177.87 dB/cm, and 211.26 dB/cm at the grating period of 490 nm, 500 nm, and 510 nm, respectively.

In Figs. 4 and 5, the (a) and (b) are represented the CL of x-polarized and y-polarized modes, respectively. And the mechanism of the two polarized are different. Specifically, the CL of x-polarized core mode is modulated by grating. And the operation principle in the y-polarized mode depends not only on grating, but also on the coupling with planar waveguide. Therefore, the changes of grating width and period lead to the liner variation at x-polarized. The adjustment of these grating

parameters also results in the change of the coupling region between the plate and the y-polarized. For example, the decrease of the grating width and the increase of the period lead to the increase of the coupling region. Based on these deductions, the trend of change in Figs. 4(b) and 5(b) are non-linear.

From what has been mentioned above, it is obvious that the changing grating parameters causes the varying of the CL in the both x-polarized mode and y-polarized mode. It can be explained by (8) and (10). From (8), it is quite clearly that the maximum loss of x-polarized core mode is modulated by grating. And the basic operation principle in the y-polarized mode is essentially related to the coupling with planar waveguide. Specifically, the optimizing of grating parameters leads to the adjusting of coupling with planar waveguide.

### B. Influence of Metal Plana $Mt$

The metal grating has an important impact on the performance of the device. Besides, an effective thickness of the metal plate is also one of the significate parameters to be considered. Fig. 7 gives the response of CL characteristics with the plate thickness increasing from 30 nm to 50 nm. According to Fig. 7(a), the change of  $Mt$  dose not impact on the resonance region A due to reaction mechanism in the x-polarized mode. The resonance wavelength in region B shows a subtle red-shift with  $Mt$  increasing. It is noting that the value of major-peak is decreased but sub-peak is unchanged. Another interesting fact is noticed in region B,  $Mt = 50$  nm, there is a sharp drop at the wavelength of 1339 nm. Based the derivation of (13), the sharp drop is due to the coupling between the harmonic of the grating order and the fiber core. And the illustration shows electric field intensity in the x-polarized mode. From the Fig. 7(b), the value of resonance wavelength is subtle increasing with  $Mt$  increasing. The related CLs are 177.87 dB/cm, 186.39 dB/cm, and 189.43 dB/cm at the plate thickness 30 nm, 40 nm, and 50 nm, respectively. Specifically, the y-polarized mode is mainly modulated by the plate waveguide, and the optimizing of  $Mt$  can make the resonance wavelength shift to longer wavelength.

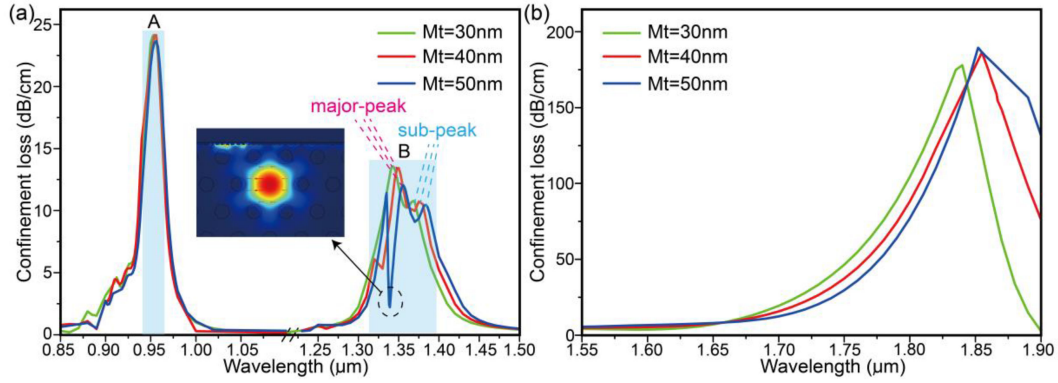


Fig. 7. The influence of metal plana on the device, Mt represents the plana thickness. (a) The confinement loss of x-polarized mode. (b) The confinement loss of y-polarized mode with varying thickness from 30 to 50 nm.

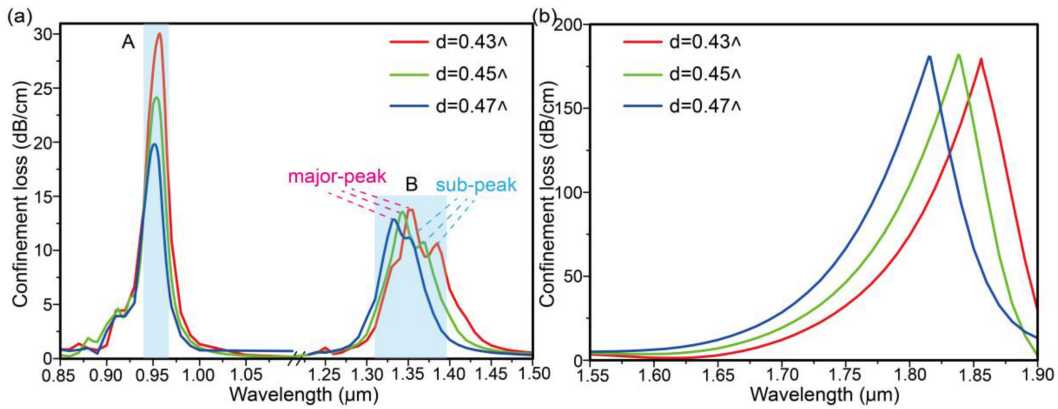


Fig. 8. The influence of structural fault,  $d/\Lambda$  represents the duty ratio. (a) The confinement loss of x-polarized mode. (b) The confinement loss of y-polarized mode with varying distances of air holes from  $0.43\Lambda$  to  $0.47\Lambda$ .

The vector matching detuning ( $\varpi$ ) mentioned in (8) is related to the grating and metal plane. Specifically, the change of grating width (a) and plane thickness (Mt) have a subtle effect on the detuning. It is noting that the grating period (t) has a great influence on the detuning, as seen in the Fig. 6. The distinct increase phenomenon of the resonant wavelength difference is accompanied by the change of loss difference with the grating period increasing.

### C. Influence of Structural Fault Tolerance $d/\Lambda$

To further analyze its performance stability, we have simulated the fault-tolerant of the MOF. Considering the effect of the preparation process on the air holes, we simulate three cases with duty ratio ( $d/\Lambda$ ) of 0.43, 0.45, and 0.47. The influence of the duty ratio is shown in Fig.8. From the Fig.8(a), the corresponding resonance wavelength in region A has unchanged but the peak value is significantly decreased and with  $d/\Lambda$  increasing from 0.43 to 0.47. It is worth noting that the CL becomes complexity in region B. The resonance wavelength shows a blue shift, and the peak value of major-peak is decreased and sub-peak is unchanged. According to Fig. 8(b), the unchanged of resonance peak value is accompanied by a blue shift.

### D. The Controllable Polarizing Performance

To optimize optical properties, we simulate the parameters of the grating height Hm. Fig. 9 shows the CL of the device in regards to Hm variations from 200 to 400 nm, and the distance between the metal plate and the core is fixed. As the height of the grating increasing, the distance between the grating and the fiber core is decreased. It is to be noticed that the deeper height produces more wave vector components. That is why the CL becomes complicated. From Fig. 9(a), the distinct red shift of the resonant wavelength is accompanied by the appearance of harmonic peaks. Moreover, the corresponding peak values significantly increases and the number of resonant wavelengths has increased with Hm changing from 200 to 400 nm. Specifically, we divide the CL into five regions (A, B, C, D, E), the resonant wavelength at shows a shift from A to B to C. And the peak value of 24.15 dB/cm is significantly increased with increasing Hm and reaches the value of 37.24 dB/cm for 400 nm. The resonant wavelength at also has been a shift from C to D to E, and the peak values are about 13.35 dB/cm, 63.12 dB/cm, and 92.62 dB/cm, respectively.

According to Fig. 9(b), it is worth noting that the height changing does not impact on the location of the major peak (in region E). But the peaks value of resonant wavelength is found

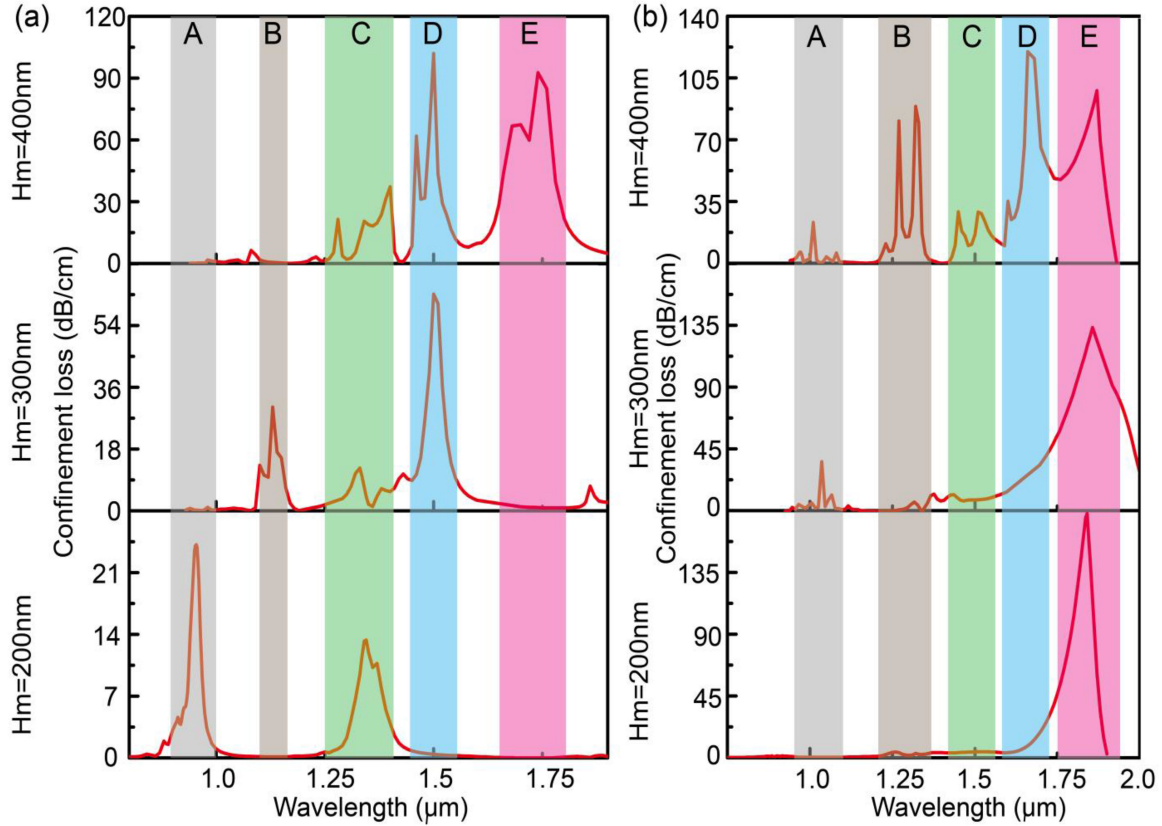


Fig. 9. The influence of grating height on the device, Hm represents the grating height. (a) The confinement loss of x-polarized mode. (b) The confinement loss of y-polarized mode with varying Hm from 200 to 400 nm.

to be 177.87 dB/cm, 134.08 dB/cm, and 97.84 dB/cm for Hm = 200 nm, 300 nm, and 400 nm. Besides, at Hm = 300 nm, there is a new resonant wavelength in region A, and at Hm = 400 nm, the new resonant peaks appear in region B, C, and D.

From the analyses above with different height, it is quite clear that the deeper height causes increment in the number of resonant wavelengths in the both x-polarized mode and y-polarized mode. The core mode in the orthogonal direction can be dual-modulated by changing Hm. Hence, we could control the resonance wavelengths to appear in a specific region and its polarization characteristics.

#### IV. ANALYSIS OF CROSSTALK CHARACTERISTICS IN DIFFERENT WAVEBANDS

Crosstalk (CT) is also an important parameter to evaluate polarizing performance, and it can be described as follow (15):

$$CT = 20\log_{10} \exp[(\alpha_2 - \alpha_1)L] \quad (15)$$

Where  $\alpha_1$  and  $\alpha_2$  express CT in x-polarized mode and y-polarized mode respectively, and L presents the length of MOF [22]. The CT spectra is plotted in Fig. 10. At different grating heights, the absolute value of CT is distinct increased with the fiber length increasing. Fig. 10(c) shows the CT for the height of 200 nm, there are three obvious peaks due to the different regions of resonance wavelength in x-polarized mode and y-polarized

mode. Maximum 1543.7 dB of CT is achieved when L is 10 mm. And Fig. 10(a), (b) show the CT spectra for the height of 400 nm and 300 nm. Maximums of CT are achieved 771.8 dB and 1234.9 dB at 400 nm and 300 nm of the grating height, respectively. Specifically, the numbers of CT wavelengths are significantly increased with the optimizing of height from 200 nm to 400 nm. Therefore, the device can filter the x-polarized mode or y-polarized mode in a specific waveband. It is quite clear that the metal DMFP can effectively adjust the number of resonance wavebands, and then realize multi-wavelength polarization filtering.

Finally, Table I summarizes the characteristics of polarizers reported in recent years, including liquid-filled, metal-coated and Gold-coated PCF. We may find that each polarizer shows advantages in one or two parameters. While, the device in this work has the performance of broadening tunable polarization, which is not available in previous devices. And the articles on D-shaped grating PCF in recent years has been summarized in the Table II. This paper mainly studies the special properties of grating periodicity which has never been mentioned in previous articles. The device can realize the function of bi-direction multi-band polarization filtering and the corresponding wavelengths of polarizing filtering are related with the period of grating. And, the device can obtain the broaden tunable polarizing filter by optimizing the structure of metal grating.

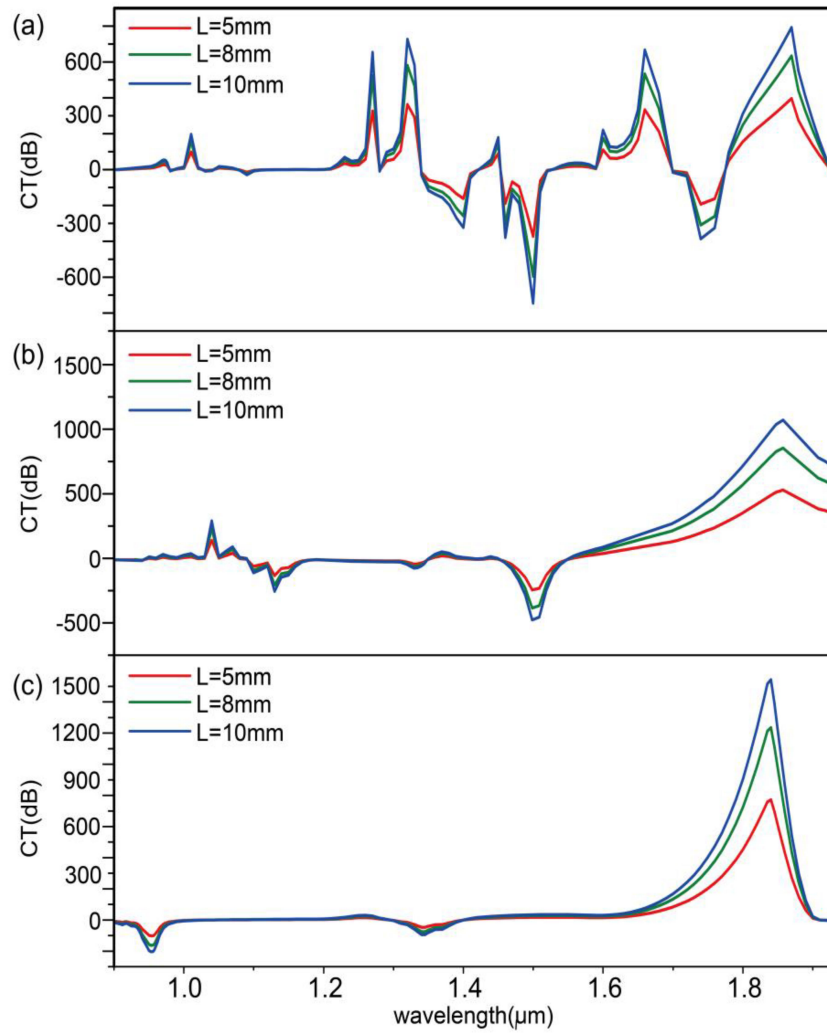


Fig. 10. The dependence of crosstalk on the wavelength. (a) Hm is 400 nm. (b) Hm is 300 nm. (c) Hm is 200 nm.

TABLE I  
POLARIZATION PERFORMANCE OF POLARIZERS

Optical structure and ref.	Polarization direction and number	Resonance loss (dB/cm)	CT ( dB L = 1 mm )
Liquid-Filled PCF [12]	y-pol one	508	NA
Metal-Coated PCF [13]	y-pol one	452.4	181 ( L = 4 mm )
Gold-Coated holes PCF [14]	x-pol one	771.5	NA
Gold-Coated in large holes PCF [15]	x-pol one	369	290
	y-pol one	475	407
Metal-Filled PCF [16]	x-pol two	251.26	212
	y-pol two	224.44	198
Metal-Coated PCF [17]	x-pol multiple	265.04	107
	y-pol multiple	230.5	95
Metal Grating DMOF [ this work ]	x-pol multiple	101	74.49
	y-pol multiple	119.94	79.24

( Hm = 400 nm, max )



TABLE II  
FUNCTION OF D-SHAPE GRATING PCF

Materials taken	wavelength (um)	function
Ag-TiO <sub>2</sub> [23]	0.5-1.2	one-direction sensor
Ag-SnO <sub>2</sub> [23]	0.5-1.2	one-direction sensor
Ag-TiO <sub>2</sub> [24]	0.5-0.64	one-direction sensor
Au [25]	1.5-1.7	one-direction sensor
Au [26]	1.4-1.8	one-direction sensor
Au [this work]	x-pol 0.35-1.6 y-pol 1.55-1.9	bi-direction multi-wavelength filter

## V. CONCLUSION

In this paper, we presented a metal grating-assisted D-shaped MOF filter for multi-polarization filtering. The simulation results show that the x-polarized core mode is periodically modulated by the grating easily. Additionally, numerical results illustrate that the metal grating exhibits a significant effect on the resonance wavelength, and the core mode can capture abundant wave vector of grating via optimizing Hm. Therefore, the new coupling method can generate more polarization wavebands and break the limitation of single mode coupling. Besides, the CT can reach to 1543.7 dB for the height of 200 nm. These excellent results indicate the device can realize multi-wavelength polarization filtering. We believe that the optical polarizing characteristics combined metal grating and MOF has great potentials in optical filtering, communication, functional devices, etc.

## REFERENCES

- [1] J. Liu *et al.*, "ZnS nanospheres for optical modulator in an erbium-doped fiber laser," *Annalen der Physik*, vol. 532, 2020, Art. no. 1900454.
- [2] Y. Huang *et al.*, "Tunable electro-optical modulator based on a photonic crystal fiber selectively filled with liquid crystal," *J. Lightw. Technol.*, vol. 37, no. 9, pp. 1903–1908, 2019.
- [3] Z. Xie *et al.*, "Integrated (de)multiplexer for orbital angular momentum fiber communication," *Photon. Res.*, vol. 6, no. 7, pp. 734–749, 2018.
- [4] C. Zou *et al.*, "Single/dual-wavelength switchable bidirectional Q-switched all-fiber laser using a bidirectional fiber polarizer," *Opt. Lett.*, vol. 43, no. 19, pp. 4819–4822, 2018.
- [5] S. Chen, F. Tian, L. Li, H. Qu, Z. Su, and J. Zhang, "Double D-shaped hole optical fiber coated with graphene as a polarizer," *Appl. Opt.*, vol. 57, no. 28, pp. 7659–7666, 2018.
- [6] K. Minn, B. Birmingham, B. Ko, H. W. H. Lee, and Z. Zhang, "Interfacing photonic crystal fiber with a metallic nanoantenna for enhanced light nanofocusing," *Photon. Res.*, vol. 9, no. 2, pp. 252–258, 2021.
- [7] V. K. Sharma and D. Kumar, "Effect of buffer layer index on short range surface plasmon polariton based TE pass polarizer," *Eng. Res. Exp.*, vol. 2, 2020, Art. no. 045031.
- [8] Y. Zhu *et al.*, "Hybrid plasmonic graphene modulator with buried silicon waveguide," *Opt. Commun.*, vol. 456, 2020, Art. no. 124559.
- [9] M. Z. Alam, S. J. Aitchison, and M. Mojahedi, "Compact and silicon-on-insulator-compatible hybrid plasmonic TE-pass polarizer," *Opt. Lett.*, vol. 37, no. 1, pp. 55–57, 2012.
- [10] X. Sun, M. Mojahedi, and J. S. Aitchison, "Hybrid plasmonic waveguide-based ultra-low insertion loss transverse electric-pass polarizer," *Opt. Lett.*, vol. 41, no. 17, pp. 4020–4023, 2016.
- [11] X. Wang, J. Lin, W. Sun, Z. Tan, R. Liu, and Z. Wang, "Polarization selectivity of the thin-metal-film plasmon-assisted fiber-optic polarizer," *ACS Appl. Mater. Interfaces*, vol. 12, pp. 32189–32196, 2020.
- [12] J. Xue, S. Li, Y. Xiao, W. Qin, X. Xin, and X. Zhu, "Polarization filter characters of the gold-coated and the liquid filled photonic crystal fiber based on surface plasmon resonance," *Opt. Exp.*, vol. 21, no. 11, pp. 13733–13740, 2013.
- [13] Q. Liu *et al.*, "Broadband single-polarization photonic crystal fiber based on surface plasmon resonance for polarization filter," *Plasmonics*, vol. 10, pp. 931–939, 2015.
- [14] H. Li, S. Li, H. Chen, J. Li, G. An, and J. Zi, "A polarization filter based on photonic crystal fiber with asymmetry around gold-coated holes," *Plasmonics*, vol. 11, pp. 103–108, 2015.
- [15] J. Zi, S. Li, H. Chen, J. Li, and H. Li, "Photonic crystal fiber polarization filter based on surface plasmon polaritons," *Plasmonics*, vol. 11, pp. 65–69, 2015.
- [16] X. Lu, M. Chang, N. Chen, X. Zhang, S. Zhuang, and J. Xu, "Design of a metal-filled photonic-crystal fiber polarization filter based on surface plasmon resonance at 1.31 and 1.55 um," *IEEE Photon. J.*, vol. 10, no. 5, May 2018, Art. no. 7203913.
- [17] B. Li, M. Li, L. Peng, G. Zhou, Z. Hou, and C. Xia, "Research on dual-wavelength single polarizing filter based on photonic crystal fiber," *IEEE Photon. J.*, vol. 9, no. 4, Apr. 2017, Art. no. 5700209.
- [18] M. Seo, J. Lee, and M. Lee, "Grating-coupled surface plasmon resonance on bulk stainless steel," *Opt. Exp.*, vol. 25, no. 22, pp. 26939–26949, 2017.
- [19] B. Li *et al.*, "Design and characterization of bio-chemical sensor based on photonic crystal fiber with fluorine-doped tin oxides film," *Plasmonics*, vol. 14, pp. 197–203, 2018.
- [20] A. Vial, A.-S. Grimault, D. Macías, D. Barchiesi, and M. L. de la Chapelle, "Improved analytical fit of gold dispersion: Application to the modeling of extinction spectra with a finite-difference time-domain method," *Phys. Rev. B*, vol. 71, 2005, Art. no. 085416.
- [21] A. A. Rifat, R. Ahmed, G. A. Mahdiraji, and F. R. M. Adikan, "Highly sensitive D-shaped photonic crystal fiber-based plasmonic biosensor in visible to Near-IR," *IEEE Sensors J.*, vol. 17, no. 9, pp. 2776–2783, Sep. 2017.
- [22] B. Li *et al.*, "Surface plasmon resonance on the V-type microstructured optical fiber embedded with dual copper wires," *Plasmonics*, vol. 14, pp. 383–387, 2018.
- [23] S. K. Dubey, A. Kumar, A. Kumar, A. Pathak, and S. K. Srivastava, "A study of highly sensitive D-shaped optical fiber surface plasmon resonance based refractive index sensor using grating structures of Ag-TiO<sub>2</sub> and Ag-SnO<sub>2</sub>," *Optik*, vol. 252, 2020, Art. no. 168527.
- [24] H. R. Fang, C. J. Wei, H. R. Yang, B. Zhang, L. Yuan, and J. Li, "DShaped photonic crystal fiber plasmonic sensor based on silver titanium dioxide composite micrograting," *Plasmonics*, vol. 16, pp. 2049–2059, 2021.
- [25] T. Khanikar and V. K. Singh, "Gold grating assisted SPR based dshaped single mode fiber for detection of liquid refractive index," *Plasmonics*, vol. 51, 2019, Art. no. 296.
- [26] J. J. Lu, Y. Li, Y. H. Han, Y. Liu, and J. M. Gao, "D-shaped photonic crystal fiber plasmonic refractive index sensor based on gold grating," *Appl. Opt.*, vol. 57, no. 19, pp. 5269–5272, 2018.